

Growth and characterization of conductive SrRuO₃ and LaNiO₃ multilayers on textured Ni tapes for high-J_c YBa₂Cu₃O_{7-δ} coated conductors

T. Aytug,^{a)} B.W. Kang, C. Cantoni, E.D. Specht, M. Paranthaman, A. Goyal, and D.K. Christen

Oak Ridge National Laboratory, Oak Ridge, Tennessee 37831

D.T. Verebelyi

American Superconductor Corporation, Two Technology Drive, Westborough, Massachusetts 01581

J.Z. Wu

Department of Physics and Astronomy, University of Kansas, Lawrence, Kansas 66045

R.E. Ericson and C.L. Thomas

3M Company, St. Paul, Minnesota 55144

C-Y. Yang and S.E. Babcock

Department of Materials Science and Engineering and Applied Superconductivity Center, University of Wisconsin—Madison, Madison, Wisconsin 53706

(Received 2 February 2001; accepted 2 July 2001)

Power applications of high-temperature superconducting (HTS) coated conductors will require stabilization against thermal runaway. We have developed conductive buffer layers to electrically couple the HTS layer to the underlying metal substrate. The structure comprises the layer sequence of SrRuO₃ (SRO) on LaNiO₃ (LNO) on biaxially textured Ni substrates. We report baseline investigations of compatibility of SRO/LNO multilayer structure with processing of YBa₂Cu₃O_{7-δ} (YBCO) and demonstrate biaxially textured YBCO films on conductively buffered Ni tapes. These YBCO coatings exhibit self-field J_c values as high as 1.3 × 10⁶ A/cm² at 77 K, and the entire structure (HTS + conductive buffers + metal substrate) shows good electrical connectivity. These results demonstrate that SRO/LNO buffer layers may provide a basis for stabilized coated conductors.

I. INTRODUCTION

The recently developed process of rolling-assisted biaxially textured substrates (RABiTS) has emerged as a viable technique for the fabrication of long-length high-temperature superconducting wires (HTS coated conductors).^{1,2} These HTS coated conductors, formed on Ni and/or Ni-alloy substrates, would enable high-current and high-magnetic-field applications operating at liquid-nitrogen temperatures. The technique employs simple, well established, and industrially scalable thermomechanical processing to obtain sharp biaxially cube-textured metal tapes that can be produced over long lengths. These biaxially textured metallic substrates

serve as templates for the deposition of epitaxial buffer layers that provide a barrier to chemical interactions with Ni and at the same time yield chemically and structurally compatible surfaces for the epitaxial growth of HTS films.

Major potential applications of HTS coated conductors involve the efficient production, distribution, and storage of electrical power. Ideally, for these applications conductive-oxide buffer layers are preferred as they can provide an electrical contact between the thin HTS layer and the thick underlying metal substrate. This electrical coupling reduces the overall resistivity and, consequently, improves the electrical and thermal stability of the entire structure (HTS + conductive buffers + metal substrate) in the event of a transient to the dissipative regime. To date however, buffer-layer development for coated conductors has mainly concentrated on insulating oxides and multilayers.¹⁻⁴ The development of conductive-

^{a)}e-mail: aytug@solid.ssd.ornl.gov

oxide buffer layers on RABiTS has just begun.^{5,6} Recently, we successfully demonstrated viability of the SrRuO₃/LaNiO₃ bilayer structure on single-crystal substrates [SrTiO₃ (STO) and/or LaAlO₃ (LAO)] as a possible conductive buffer-layer architecture for the growth of high critical current density (J_c) YBa₂Cu₃O_{7- δ} (YBCO) coatings.⁷

Both SrRuO₃ (SRO) and LaNiO₃ (LNO) are perovskite-type, conductive metallic oxides with pseudocubic lattice parameters of 3.93 and 3.83 Å and room-temperature resistivities of around 300 and 600 $\mu\Omega$ cm, respectively. These values are a close match to those of orthorhombic YBCO and other HTS materials. In recent years, considerable attention has focused on the fabrication of LNO and SRO films due to their potential for many technological applications. For instance, their use as electrodes on ferroelectric substrates as well as normal-metal layers in superconductor/normal-metal/superconductor Josephson junctions have been demonstrated by several groups.⁸⁻¹⁴ In addition, their potential as buffer layers for the epitaxial growth of YBCO films on various insulating, single-crystal substrates has also been investigated.^{9,15} The results of those studies and our previous work have demonstrated that high-quality epitaxial YBCO films can be grown on SRO and SRO/LNO buffered single-crystal substrates with high superconducting transition temperatures ($T_c = 90-91$ K) and high- J_c values [$(2-4) \times 10^6$ A/cm² at 77 K and self-field]. However, these studies also showed that, despite a good crystalline structure, the YBCO films grown directly on LNO buffer layers exhibit significantly lower $T_c \cong 85-89$ K and $J_c \leq 1 \times 10^6$ A/cm² values. It was found that the YBCO films suffered from Ni contamination through the LNO layers.⁷ This result was also consistent with the earlier study where YBCO films grown on highly textured LNO/Ni substrates showed depressed T_c values around 75–80 K.⁶ Although there have been no reports of successful YBCO growth on SRO single buffer layers on textured metals, the observations above suggest that the SRO/LNO bilayer structure on Ni offers promise for the development of RABiTS-based, fully conductive YBCO-coated conductors.

In this paper, we first use single-crystal oxide substrates (STO and LAO) to investigate the chemical compatibility of LNO and SRO/LNO multilayers with the YBCO films, including studies of the electrical properties and thermal compatibility of SRO/LNO bilayers under the growth conditions used for YBCO films. Second, we report for the first time the successful fabrication of a conductive buffer-layer RABiTS structure, employing the layer sequence of SRO/LNO on biaxially textured Ni tapes. The structural and superconducting properties of YBCO films grown on these buffered Ni substrates are reported.

II. EXPERIMENTAL

Two different procedures were used for the deposition of SRO/LNO multilayers on Ni and on STO or LAO single-crystal substrates. For the Ni substrates, rf-magnetron sputtering was used for deposition of both the base LNO and the top SRO layers. The sputter targets used for these experiments were made from single-phase LNO and SRO powders, prepared by solid-state synthesis, which were lightly packed into a copper target tray. Deposition of LNO base layers was accomplished at substrate temperatures (T_{dep}) ranging from 450 to 500 °C. To suppress the formation of NiO, and to achieve (001)-oriented epitaxy directly on the Ni(001) surface, a reducing atmosphere of forming gas (96% Ar + 4% H₂) was used at the initial stages of LNO growth (approximately 2–3 min), followed by deposition in oxidizing conditions at a total pressure of 10 mtorr. The H₂ partial pressure ensures the instability of NiO during the initial nucleation of the LNO layer. The deposition rate was approximately 0.42 Å/s, and the resulting LNO film thickness was 300 nm. Subsequent growth of SRO films on LNO/Ni substrates was performed at a substrate temperature in the range of 600–650 °C under 10 mtorr of Ar. The deposition rate for SRO was 0.48 Å/s with the corresponding film thickness of 400 nm.

Deposition of LNO and SRO buffer layers on STO and LAO single-crystal substrates was conducted by a combination of rf-magnetron sputtering and pulsed-laser deposition (PLD), respectively. Typical sputtering conditions for LNO consisted of a mixture of Ar and O₂ at a ratio of Ar/O₂ = 15/2, with a total pressure of 10 mtorr, and a substrate temperature in the range 550–600 °C. The SRO layers were deposited using a KrF excimer-laser ablation system operated with an energy density of approximately 3 J/cm². During the deposition of SRO layers the substrates were kept at 600 °C in an O₂ atmosphere of 5 mtorr. Typical film thicknesses for these LNO and SRO layers were around 300 and 200 nm, respectively.

The PLD technique was also employed for deposition of the YBCO films on buffered single-crystal and Ni substrates, where a laser energy density of approximately 4 J/cm² was used. During deposition of the YBCO films, the buffered substrates were kept at 780 °C in the presence of an O₂ pressure (P_{O_2}) around 120 mtorr. After deposition, the samples were first cooled to 600 °C at a rate of 5 °C/min; then the O₂ pressure was increased to 550 torr, and the samples were cooled to room temperature at the same rate. The deposition rate was approximately 3.3 Å/s, and typical film thicknesses of YBCO coatings were 200 nm. Film crystal structures were characterized with a Huber high-resolution x-ray diffractometer (XRD), and microstructural analyses were conducted using two different types of scanning electron

microscopes (SEM). For the surface morphology observations a JOEL model JSM-840 SEM was used, and for the cross-sectional observations a high-resolution field-emission type SEM (HRSEM) was applied. A standard four-probe technique was used to evaluate the electrical properties, including T_c , and J_c of the YBCO films, as well as the temperature-dependent resistivity of the conductive buffer layers. For those measurements, electrical contacts of silver were deposited onto the samples using dc-magnetron sputtering followed by O₂ annealing in 1 atm for 30 min at 500 °C. Values of J_c were assigned at a 1 μ V/cm criterion. Secondary ion mass spectrometry (SIMS) depth-profile analyses were made to document the chemical compatibility of the multilayers as related to the possible cation contamination of YBCO.

III. RESULTS AND DISCUSSION

A. Chemical compatibility of YBCO/SrRuO₃/LaNiO₃ and electrical property characterizations of SrRuO₃/LaNiO₃ bilayers on insulating single-crystal substrates

For potential applications involving a conductive interface, it is important to understand the chemical compatibility of YBCO films with the SRO/LNO structure. In addition, it is necessary to evaluate the electrical properties and the thermal compatibility of SRO/LNO bilayers under the growth conditions used for YBCO films ($T_{\text{dep}} = 780$ °C, $P_{\text{O}_2} = 100$ –200 mtorr). For the former issue, YBCO films were grown epitaxially on LNO/STO and SRO/LNO/STO multilayers, and the chemical compatibility between the YBCO and the conductive buffer layers was examined by SIMS depth-profile measurements. Figures 1(a) and 1(b) compare the results on YBCO/LNO/STO and YBCO/SRO/LNO/STO, respectively. Both samples show well-resolved interfaces and well-defined layers. For the YBCO/LNO/STO structure, a significant presence of Ni in the YBCO layer was observed, while the Ni signal for the YBCO/SRO/LNO/STO sample remains at the noise level within the YBCO. The former observation implies contamination of YBCO with Ni from the LNO layer, whereas the latter result indicates passivation of this diffusion by an additional SRO layer. These SIMS results are in accordance with our previous observations where YBCO films deposited directly on LNO buffers exhibited an increased normal state resistivity (ρ) as well as significantly lower T_c and J_c values than those of YBCO films grown on SRO/LNO bilayers.⁷ It is well documented that Ni impurities in the superconducting structure can significantly reduce T_c and increase ρ .¹⁶

To better understand the effects of YBCO deposition conditions on the conductive buffer-layer properties, two as-grown SRO/LNO/LAO epitaxial structures were annealed at various temperatures (T_{ann}) up to 780 °C

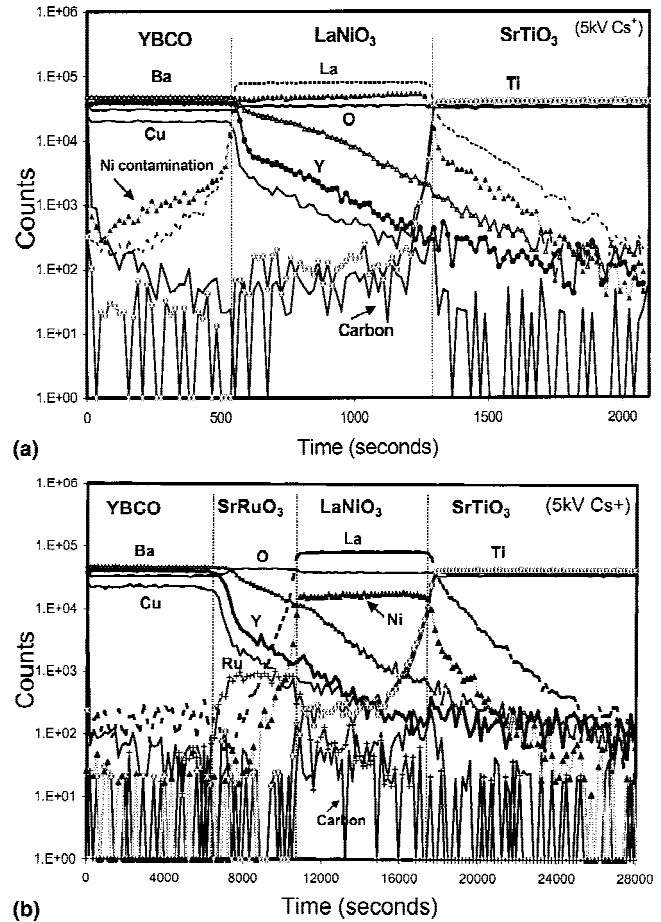


FIG. 1. SIMS depth profiles for (a) YBCO/LNO/STO and (b) YBCO/SRO/LNO/STO multilayer structures. Note that due to interference between the Sr and Ti yields, data for Sr are omitted from the depth profiles.

under fixed oxygen pressures of either 200 mtorr or 1 atm. The resulting temperature-dependent normalized resistivities, $\rho(T)/\rho(290 \text{ K})$, are plotted in Figs. 2(a) and 2(b) for the samples annealed in 200 mtorr and 1 atm, respectively. The insets of these figures give the absolute resistivity values at room temperature ($T = 290 \text{ K}$). In both samples, the value of $\rho(T = 290 \text{ K})$ for the as-grown SRO/LNO is approximately 1000 $\mu\Omega \text{ cm}$ and decreases with increasing T_{ann} . At $T_{\text{ann}} = 780$ °C, both samples show about a 50% reduction in $\rho(T = 290 \text{ K})$, with its value decreasing to around 500 $\mu\Omega \text{ cm}$, which is comparable to that of YBCO films. The higher resistivities for the as-grown samples are probably associated with their poor crystallinity arising from oxygen deficiency, impurity inclusions, or structural defects that can result from the deposition conditions of low temperatures (600 °C) and low oxygen partial pressures (2–5 mtorr). Accordingly, the as-grown samples show a metallic ρ – T behavior down to temperatures of about 40 K, below which $\rho(T)$ exhibits an upward turn that is characteristic of localization effects. With progressive annealing in

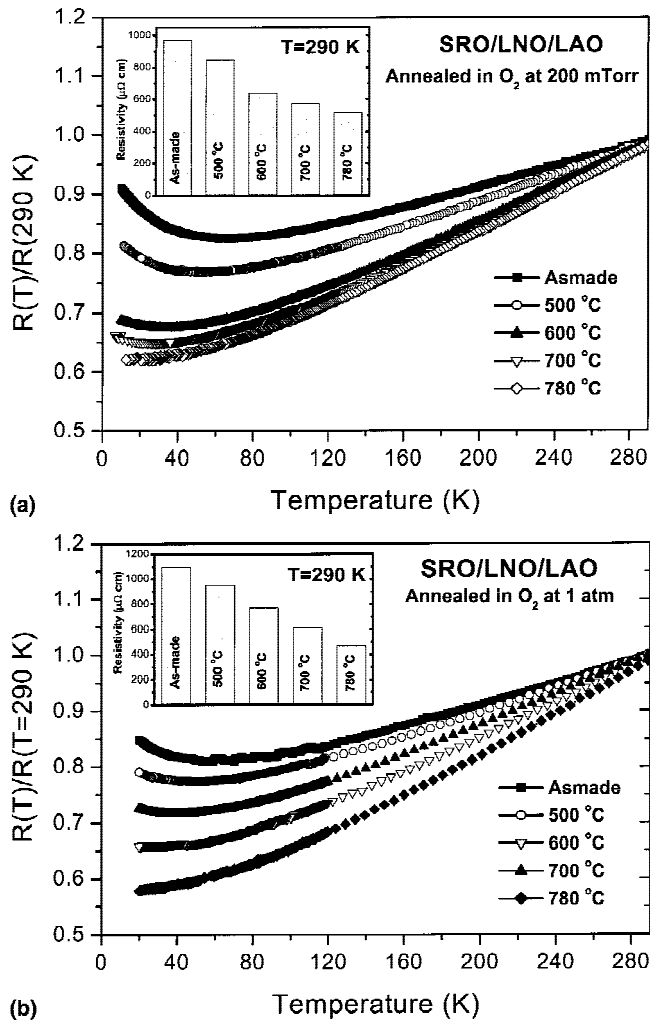


FIG. 2. Temperature dependence of normalized resistivity for SRO/LNO conductive bilayer structures annealed in oxygen pressures of (a) 200 mtorr and (b) 1 atm, at the indicated temperatures. The insets show the room-temperature resistivities of the same samples after each anneal.

oxygen, the samples show an improved metallic behavior, as evidenced by the gradual increase in residual resistivity ratio, ($RRR \equiv \rho_{290K}/\rho_{20K}$), and less pronounced low-temperature localization. It is well known that the RRR is a reflection of the film perfection. Thus, the observed increase in RRR values from 1.13 [sample in Fig. 2(a)] and 1.17 [sample in Fig. 2(b)] for the as-grown to 1.6–1.7 for the 780 °C annealed samples indicated reduced defect density and better atomic ordering for the SRO/LNO bilayer annealed at higher temperatures and higher oxygen pressures. The results of annealing studies imply that there is no remarkable dependence of the annealed SRO/LNO resistivity on postannealing oxygen pressure and provide a basis for the expected behavior prior to and during the YBCO deposition. The data

suggest that a postdeposition annealing step for the conductive buffer layers should not be necessary prior to YBCO deposition.

B. Microstructural and electrical properties of YBCO films on SrRuO₃/LaNiO₃ buffered Ni substrates

After establishing excellent chemical compatibility of YBCO films with the SRO/LNO structure and conducting electrical property characterizations of SRO/LNO bilayers, we devoted our efforts to implement the same conductive structures on Ni substrates. A typical XRD θ - 2θ scan for a 200-nm-thick YBCO film deposited on a SRO/LNO/Ni multilayer structure is shown in Fig. 3(a). The presence of only (00 l) reflections indicates that YBCO is oriented with its c axis normal to the plane of the substrate. Figure 3(b) illustrates the high-resolution XRD spectrum in the vicinity of the YBCO (006) diffraction peak to view clearly the x -axis orientation for the SRO and LNO layers as well. After YBCO deposition, a small impurity peak appeared at around 37° , which is indexed as belonging to (111) reflection of NiO. The consequence and the details of this observation are discussed later. According to the high-resolution XRD scans, the lattice parameters for YBCO, SRO, and LNO are found to be consistent with those of the bulk materials. The lattice parameters for the YBCO film are $a = 3.817 \text{ \AA}$, $b = 3.882 \text{ \AA}$, and $c = 11.69 \text{ \AA}$, and the pseudocubic lattice parameters " a_0 " for SRO and LNO are 3.956 and 3.862 \AA , respectively. To confirm the epitaxial growth and crystallinity of YBCO/SRO/LNO on Ni, XRD out-of-plane (ω -rocking curve) and in-plane (ϕ -scan) studies were carried out. The out-of-plane crystallographic texture for the YBCO, SRO, LNO, and Ni can be seen from Fig. 4. Due to the coarse-grain nature of the rolled-textured substrate, the rocking curve for the Ni shows a significant amount of structure. The ω -rocking curve scans obtained through the (002) peak reflections for Ni, LNO, and SRO and the (006) reflection for YBCO yield peak-width FWHM values ($\Delta\omega$) of 6.5° , 6.4° , 5.3° , and 4.7° , respectively, indicating progressive improvement for subsequent layers. The sharpening of the out-of-plane texture may be attributed to two possibilities: (1) gradual decrease in lattice mismatch among consecutive layers, i.e., from 9.65% for LNO–Ni to 1.7% for YBCO–SRO; (2) planar alignment with smoother surface rather than direct out-of-plane epitaxy. This high degree of out-of-plane texture is especially important as a factor in achieving high- J_c values. An important effect of this sharpening is to minimize the total grain-boundary misorientation angle, which is known to suppress J_c with an approximately exponential dependence.^{17,18} The level of in-plane crystallographic alignment and the epitaxy between individual layers of the YBCO/SRO/LNO/Ni structure are determined by ϕ -scans through the

YBCO(103), SRO(111) + LNO(111), and Ni(111) peak reflections, as shown in Fig. 5. It reveals four equally spaced peaks, separated by 90° with similar in-plane FWHM values ($\Delta\phi$) of about 10°, indicating good-quality

epitaxy among the oxide layers as well as with the underlying metal substrate. Because the Bragg angles for the SRO(111) and LNO(111) peak reflections are very similar, it was not possible to distinguish them within the resolution

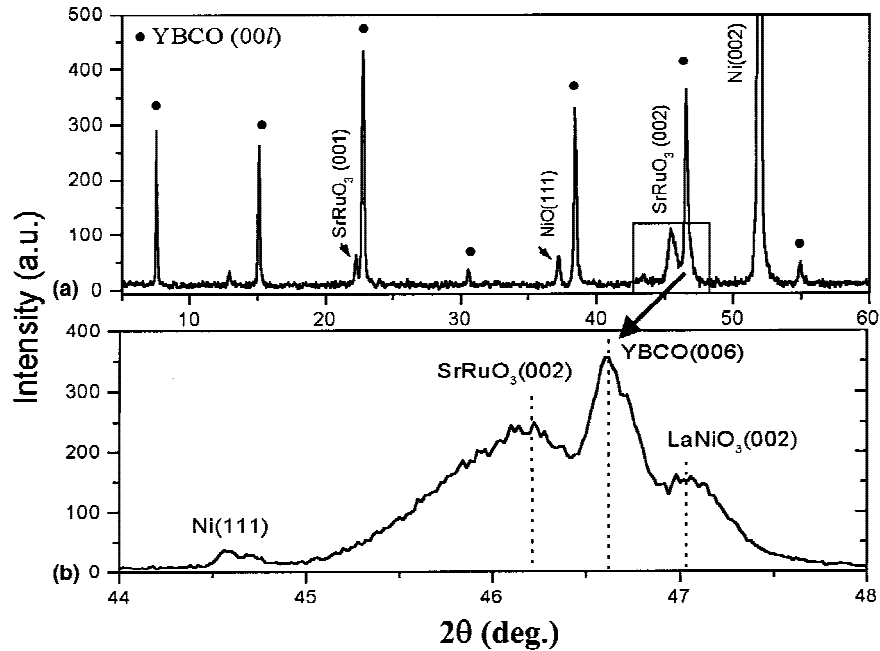


FIG. 3. XRD θ - 2θ scans for YBCO/SRO/LNO/Ni multilayer. (a) Full-range scan. YBCO (00l) peaks are indicated by (●). (b) High-resolution expanded view of the boxed region.

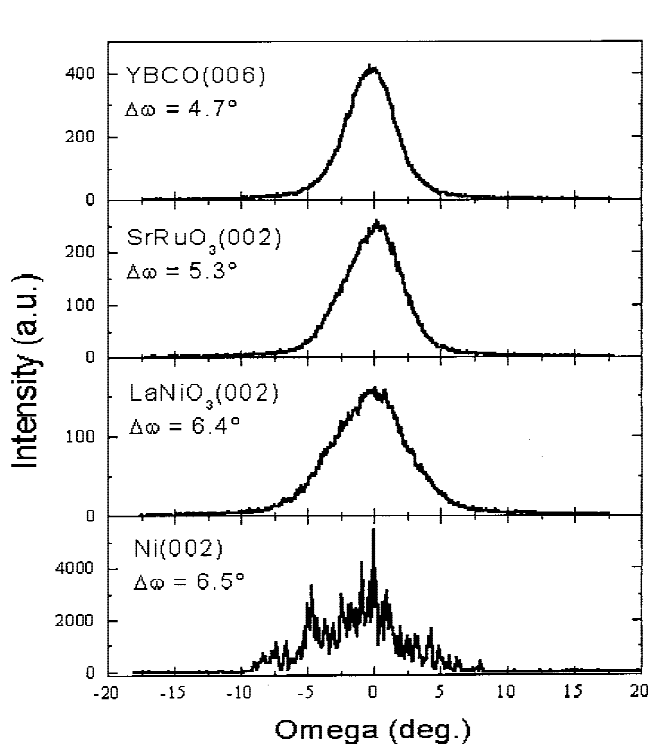


FIG. 4. XRD ω -rocking curves for the YBCO/SRO/LNO/Ni structure showing the progressive improvement of the out-of-plane texture in subsequent layers.

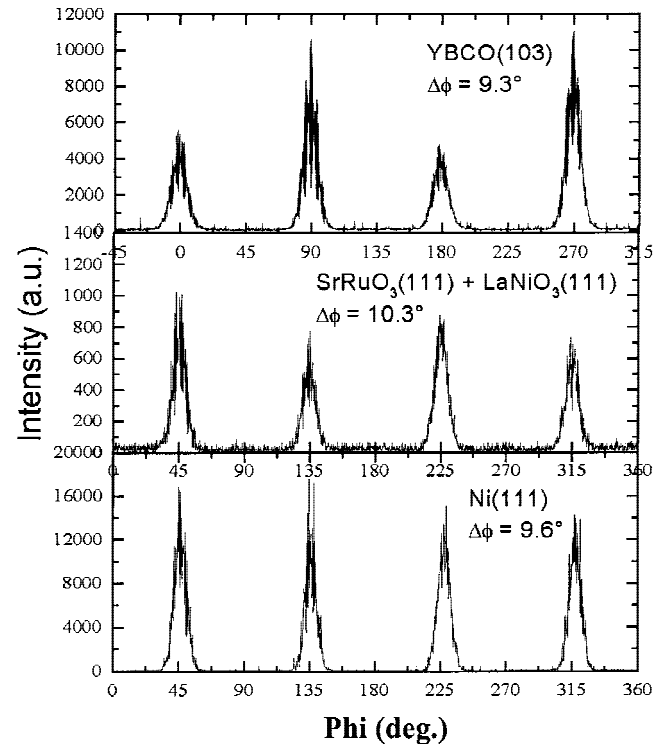


FIG. 5. XRD ϕ -scans for the YBCO/SRO/LNO/Ni structure showing that the buffer layers and YBCO tend to replicate the in-plane texture of the Ni substrate.

of our XRD system. Note that the apparent 45° rotation of YBCO with respect to the buffer layers and Ni substrate is due to the scanning of YBCO(103) reflection. In fact, all layers assume the following cube-on-cube orientation: out-of-plane YBCO[001]//SRO[001]//LNO[001]//Ni[001]; in-plane YBCO[110]//SRO[110]//LNO[110]//Ni[110]. There is no indication of any additional misoriented domains, which are undesirable due to the potential disruption of current flow by high-angle grain boundaries.

To assess the surface quality of these films, plan-view SEM micrographs of the surface morphology for a SRO/LNO/Ni multilayer structure before and after YBCO deposition are presented in Figs. 6(a) and 6(b), respectively. Figure 6(a) shows a grain-boundary region for the SRO/LNO/Ni multilayer structure. The sample has uniform, smooth, and dense morphology with excellent coverage at the Ni grain boundaries. Such a surface morphology should be realized in order to obtain high-quality YBCO films. Figure 6(b) illustrates the SEM micrograph of the YBCO film deposited on the same SRO/LNO/Ni substrate. The YBCO film also exhibits a

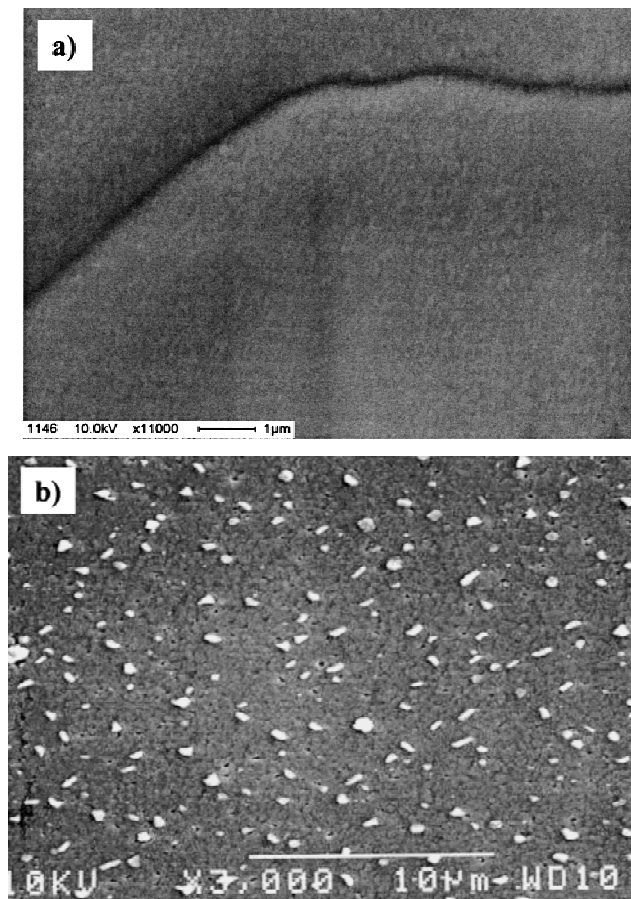


FIG. 6. SEM micrographs of (a) the grain boundary region of SRO/LNO/Ni structure and (b) the surface morphology of the YBCO film grown on the same conductive buffer structure shown in part (a).

smooth and uniform microstructure, with dense coverage very similar to that of the YBCO films deposited on SRO/LNO-buffered STO or LAO substrates. The existence of small particulates on the surface is a feature of the PLD deposition process of YBCO films¹⁹ and has no adverse effect on superconducting transport properties of interest here. It should also be noticed that the YBCO films tend to fill the groove structure of the Ni grain boundaries, as evidenced by the visual disappearance of these boundaries. This probably results from the highly anisotropic, rapid basal-plane film growth nature of YBCO.²⁰

The qualifying test for overall suitability of any buffer layer structure on Ni is compatibility with the deposition of high-quality, high- J_c YBCO coatings. The T_c value for the YBCO/SRO/LNO/Ni sample was 90 K. The magnetic field dependence of the transport J_c at 77 K for the same YBCO film is shown in Fig. 7. Shown also in the plot are data for epitaxial YBCO films grown on three other substrates, i.e., on STO, on SRO/LNO buffered LAO, and on a standard insulating-oxide buffer layer RABiTS architecture of CeO₂/YSZ/CeO₂/Ni. For comparison, data for an optimized Bi-2223/Ag powder-in-tube (PIT) sample are also included. All J_c measurements were made with the field applied parallel to the c axis. At zero applied field, the YBCO/SRO/LNO/Ni sample exhibits a J_c value of 1.3×10^6 A/cm², with an irreversibility field (H_{irr}) of 7.5 T at 77 K. As evident from the figure, this J_c performance is comparable to that of epitaxial YBCO films on single-crystal STO, SRO/LNO-buffered LAO and CeO₂/YSZ/CeO₂-buffered Ni substrates and is far superior to that of optimum-quality Bi-2223/Ag PIT wires. Hence, these results, together with those obtained from microstructural investigations,

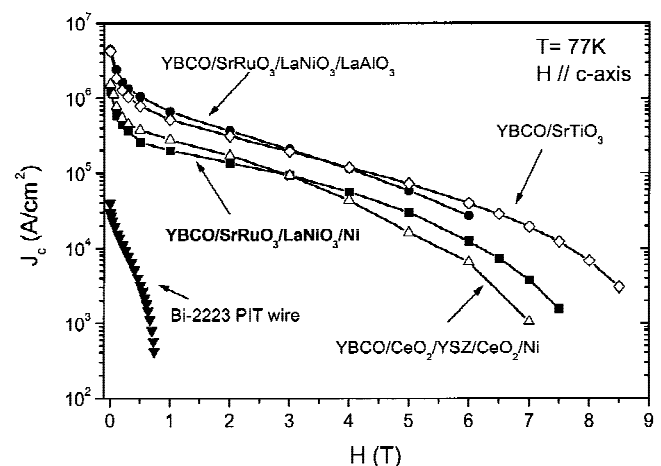


FIG. 7. Magnetic field dependence of the transport J_c , measured at 77 K, for a YBCO film on the conducting buffer structure of SRO/LNO/Ni. Also shown for comparison are $J_c(H, 77 K)$ for YBCO/STO, YBCO/SRO/LNO/LAO, YBCO/CeO₂/YSZ/CeO₂/Ni, and Bi-2223/Ag tape. For all YBCO samples, the thickness is 200 nm.

provide further support that the SRO/LNO bilayer serves as an excellent buffer-layer architecture for the development of high-quality RABiTS-based YBCO-coated conductors.

To study the electrical coupling between layers of the YBCO/SRO/LNO/Ni structure, four terminal ρ - T measurements were carried out on these samples. In Figure 8, we compare the net resistivity (ρ_{net}), which is calculated from the total thickness of the conductive structure (YBCO + buffer layers + Ni substrate), with data for the SRO/LNO/Ni multilayer, as well as with that of the bare, textured Ni substrate. It is clear that before YBCO deposition the net room-temperature resistivity of SRO/LNO/Ni is close to that of Ni ($\rho \approx 7 \mu\Omega \text{ cm}$), and both exhibit a similar ρ - T behavior, indicating good metallic contact among individual layers of SRO/LNO/Ni structure. After YBCO deposition, however, we observed a somewhat degraded metallic conductivity for the YBCO/SRO/LNO/Ni, as evidenced by the relative increase in the ρ_{net} of the structure. Similar ρ - T behavior was also observed on several other samples studied. The fact that ρ_{net} is measurably higher than that of the Ni tape implies that the YBCO/SRO/LNO composite is not ideally electrically connected to the underlying Ni substrate. While this low-level resistivity would provide significant stability, the result suggests some interaction between the buffer layers and Ni during the YBCO deposition.

To investigate this issue, cross-sectional HRSEM studies were performed on a YBCO/SRO/LNO/Ni sample and are compared to the interface for an as-grown LNO/Ni sample. These results are presented in Figs. 9(a) and in 9(b), respectively. In can be seen clearly from Fig. 9(a) that the interface between LNO and Ni is flat, sharp, and homogeneous with no evidence of interdiffusion between the buffer layer and the metal substrate or the presence of

any intermediate layers, such as NiO. After YBCO deposition, the interfaces between YBCO-SRO and SRO-LNO remain clean and homogeneous although roughening of the LNO-Ni interface is apparent from Fig. 9(b). This sample shows discontinuous NiO regions at the LNO-Ni interface, which are in accordance with the observation of a NiO(111) peak in the XRD analysis presented in Fig. 3(a). Apparently, this NiO formation results from the diffusion of oxygen through the buffer layers into the Ni substrate during the YBCO deposition. There also exists a dark nonuniform region just above the Ni interface, which suggests the possibility of some LNO decomposition. This may result from the diffusion of Ni from the metal substrate into the LNO layer at the higher temperatures and oxidizing ambients used for YBCO growth. This suggests a deterioration of the stability and hence the structural quality of the LNO layer. Recall that significant diffusion of Ni through the substrate into subsequent buffer and superconducting layers has been observed according to the results of SIMS analysis, as previously discussed in Sec. III. A. Even though we cannot determine the exact chemical nature of the interface region within the capability of our measurement techniques,

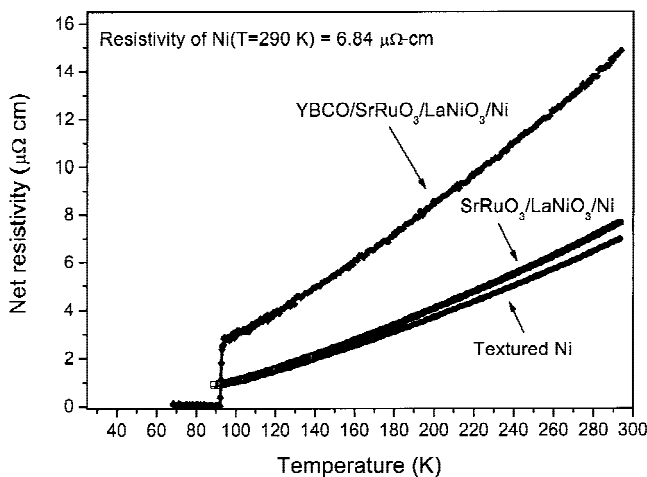


FIG. 8. Temperature-dependent net resistivity of the YBCO/SRO/LNO/Ni sample shown in the previous figure. Also shown for comparison are the ρ_{net} - T data for an as-made SRO/LNO/Ni conductive structure and for a pure biaxially-textured Ni substrate.

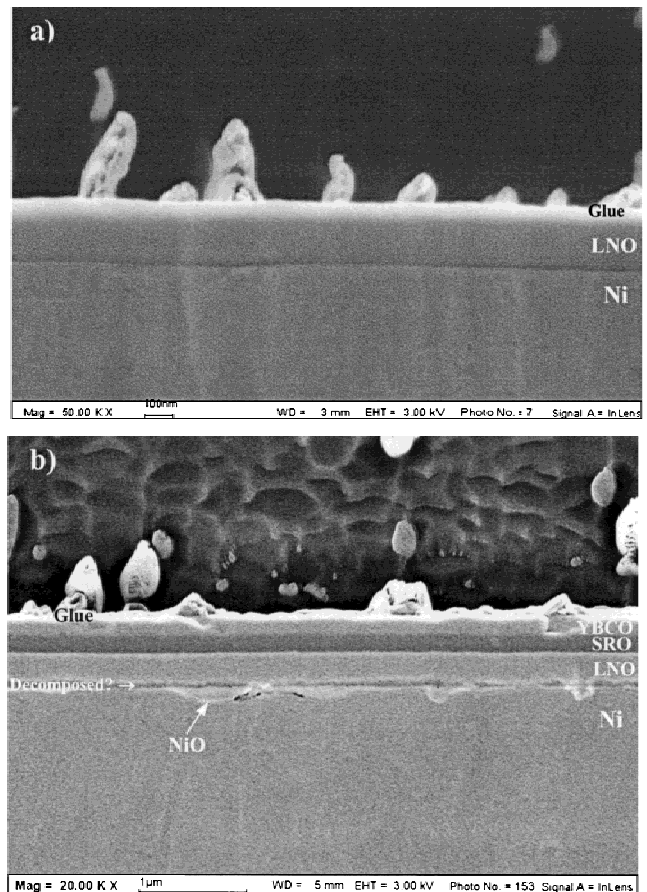


FIG. 9. Cross-sectional HRSEM micrographs of (a) LNO/Ni and (b) YBCO/SRO/LNO/Ni multilayer structures.

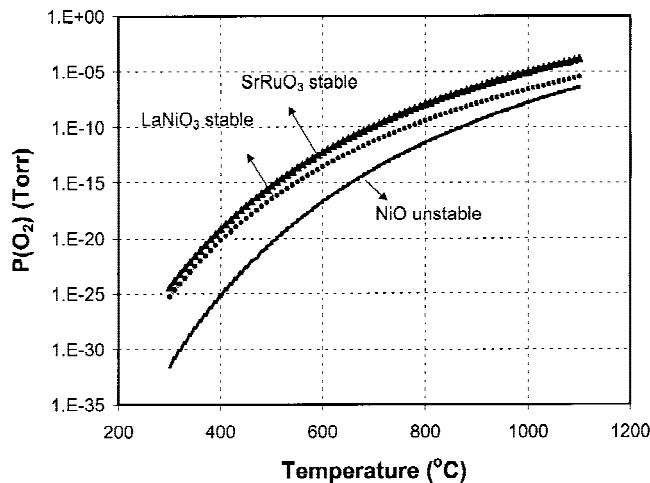


FIG. 10. Thermodynamic stability lines for SRO, LNO, and Ni for a range of temperatures and oxygen pressures, P_{O_2} , of interest.

we may speculate that it is probably composed of a polycrystalline mixture of La–O and Ni–O compounds. In fact, from thermodynamic considerations based on the bulk free energies it has been found that NiO is more stable than either SRO or LNO, as shown in Fig. 10.^{21,22} Hence, these results provide plausible evidence for the increase observed in the ρ_{net} data for the YBCO/SRO/LNO/Ni structure. Nevertheless, experimentally it appears that reasonably good metallic conductivity between the YBCO/SRO/LNO and the Ni substrate remains.

While the formation of these interfacial phases most likely results from the residence time at temperature and in oxygen during the YBCO deposition, the dependence on time has not been explored systematically. We note that the high deposition rate proposed for commercial processing of YBCO coatings should minimize this residence time and thereby help to ameliorate the problem, even for thicker YBCO coatings than explored here. For example, the laboratory conditions used for the present YBCO deposition result in a deposition time of approximately 10 min. For a commercial process at proposed deposition rates of approximately 1 $\mu\text{m}/\text{min}$ and for expected YBCO coating thickness of 2–3 μm , then the residence time is actually less than required for the present studies. On the other hand, development of an alternative buffer-layer architecture, or possibly use of an intermediate buffer layer between the SRO/LNO bilayer and Ni, could be effective to passivate the Ni and/or oxygen diffusion. Pursuit of this idea and experiments are already underway.

IV. SUMMARY AND CONCLUSION

In summary, we have presented our experimental results in the fabrication and characterization of chemically and structurally compatible conductive-oxide buffer-layer

structures for the development of YBCO coated conductors for power technologies. Both single and bilayer configurations of SRO and LNO conductive oxides have been investigated. Single-crystal LAO and STO substrates have been used to achieve a thorough understanding of the buffer-layer growth and electrical properties of LNO and SRO/LNO multilayers under the deposition conditions used for YBCO films. Our results revealed that the YBCO films on LNO buffer layers suffer from Ni contamination. However, the results also indicated that an additional SRO layer can prevent the observed low-level Ni contamination of YBCO and suggest that the SRO/LNO structure may be a potential conductive buffer-layer architecture. The results of annealing studies and electrical property characterizations revealed that there is improved conductivity upon annealing at YBCO deposition temperatures but no remarkable dependence on the postannealing oxygen pressure. Thus, the data suggested that a postdeposition annealing step for the conductive buffer layers should not be necessary prior to YBCO deposition. Utilizing the fundamental understanding obtained from single-crystal substrates, we successfully deposited biaxially oriented SRO/LNO bilayers on textured Ni substrates. The crystalline structure and the surface quality of this conductive architecture were excellent, and for the first time high-quality epitaxial YBCO films were grown on a fully conductive RABiTS structure with critical current densities exceeding $1 \times 10^6 \text{ A}/\text{cm}^2$ at 77 K in self-field. The magnetic field performance of J_c was as good as that obtained for YBCO on SRO/LNO buffered single-crystal substrates and on standard CeO₂/YSZ/CeO₂-buffered Ni substrates. Most significantly, electrical property characterizations revealed good metallic conductivity between the YBCO coatings and the Ni substrate, indicating that conductive SRO/LNO bilayers may be of great potential for large-scale power applications of YBCO-coated conductors.

ACKNOWLEDGMENTS

This work was supported by the United States Department of Energy, Division of Materials Sciences, Office of Science, Office of Power Technologies-Superconductivity Program, and Office of Energy Efficiency and Renewable Energy. The research was performed at the Oak Ridge National Laboratory, managed by U.T.-Battelle, LLC, for the United States Department of Energy under Contract No. DE-AC05-00OR22725.

REFERENCES

1. A. Goyal, D.P. Norton, J.D. Budai, M. Paranthaman, E.D. Specht, D.M. Kroeger, D.K. Christen, Q. He, B. Saffian, F.A. List, D.F. Lee, P.M. Martin, C.E. Klabunde, E. Hatfield, and V.K. Sikka, *Appl. Phys. Lett.* **69**, 1795 (1996).

2. D.P. Norton, A. Goyal, J.D. Budai, D.K. Christen, D.M. Kroeger, E.D. Specht, Q. He, B. Saffian, M. Paranthaman, C.E. Klabunde, D.F. Lee, B.C. Sales, and F.A. List, *Science* **274**, 755 (1996).
3. C.M. Carlson, J.C. Price, P.A. Parilla, D.S. Ginley, D. Niles, R.D. Blaugher, A. Goyal, M. Paranthaman, D.M. Kroeger, and D.K. Christen, *Physica C* **304**, 82 (1998).
4. M. Paranthaman, D.F. Lee, A. Goyal, E.D. Specht, P.M. Martin, X. Cui, J.E. Mathis, R. Feenstra, D.K. Christen, and D.M. Kroeger, *Supercond. Sci. Technol.* **12**, 319 (1999).
5. C. Cantoni, T. Aytug, D.T. Verebelyi, M. Paranthaman, E.D. Specht, D.P. Norton, and D.K. Christen, *IEEE Trans. Appl. Supercond.* **11**, 3309 (2001).
6. Q. He, D.K. Christen, R. Feenstra, D.P. Norton, M. Paranthaman, E.D. Specht, D.F. Lee, A. Goyal, and D.M. Kroeger, *Physica C* **314**, 105 (1999).
7. T. Aytug, J.Z. Wu, C. Cantoni, D.T. Verebelyi, E.D. Specht, M. Paranthaman, D.P. Norton, D.K. Christen, R.E. Erickson, and C.L. Thomas, *Appl. Phys. Lett.* **76**, 760 (2000).
8. C.B. Eom, R.B. Van Dover, J.M. Philips, D.J. Werder, J.H. Marshall, C.H. Chen, R.J. Cava, R.M. Fleming, and D.K. Fork, *Appl. Phys. Lett.* **63**, 2570 (1993).
9. M. Sagoi, T. Kinno, J. Yoshida, and K. Mizushima, *Appl. Phys. Lett.* **62**, 1833 (1993).
10. C.C. Yang, M.S. Chen, T.J. Hong, C.M. Wu, J.M. Wu, and T.B. Wu, *Appl. Phys. Lett.* **66**, 2643 (1995).
11. L. Antognazza, K. Char, T.H. Geballe, L.L.H. King, and A.W. Sleight, *Appl. Phys. Lett.* **63**, 1005 (1993).
12. R. Dömel, C.L. Jia, C. Copetti, G. Ockenfuss, and A.I. Braginski, *Supercond. Sci. Technol.* **7**, 277 (1994).
13. X.D. Wu, S.R. Foltyn, R.C. Dye, Y. Coulter, and R.E. Muenchausen, *Appl. Phys. Lett.* **62**, 2434 (1993).
14. P. Tiwari, X.D. Wu, S.R. Foltyn, M.Q. Le, I.H. Campbell, R.C. Dye, and R.E. Muenchausen, *Appl. Phys. Lett.* **64**, 1005 (1993).
15. K.M. Satyalakshmi, R.M. Mallya, K.V. Ramanathan, X.D. Wu, B. Brainard, D.C. Gautier, N.Y. Vasanthacharya, and M.S. Hegde, *Appl. Phys. Lett.* **62**, 1233 (1993).
16. Y. Maeno, T. Nojima, Y. Aoki, M. Kato, K. Hoshino, A. Minami, and T. Fujita, *Jpn. J. Appl. Phys.* **26**, L 774 (1987).
17. D. Dimos, P. Chaudari, J. Mannhart, and F.K. Legoues, *Phys. Rev. Lett.* **61**, 219 (1988).
18. D.T. Verebelyi, D.K. Christen, R. Feenstra, C. Cantoni, D.F. Lee, M. Paranthaman, P.N. Arendt, R.F. DePaula, J.R. Groves, and C. Prouteau, *Appl. Phys. Lett.* **76**, 1755 (2000).
19. G. Koren, A. Gupta, R.J. Baseman, M.I. Lutwyche, and R.B. Laibowitz, *Appl. Phys. Lett.* **55**, 2450 (1989).
20. D.P. Norton, D.H. Lowndes, J.D. Budai, D.K. Christen, E.C. Jones, K.W. Lay, and J.E. Tkaczyk, *Appl. Phys. Lett.* **57**, 1164 (1990).
21. C. Mallika and O.M. Sreedharan, *J. Alloys Compd.* **191**, 219 (1993).
22. O.M. Sreedharan and M.S. Chandrasekharaiah, *J. Mater. Sci.* **21**, 2581 (1986).